Instantaneous growth approximation describing the nanocrystallization process of amorphous alloys. A cellular automata model

J. S. Blázquez, V. Franco, C.F. Conde, M. Millán, A. Conde*

Dpto. Física de la Materia Condensada, ICMSE-CSIC, Universidad de Sevilla, P.O.

Box 1065, 41080, Sevilla, Spain

Abstract: A cellular automata simulation based on an instantaneous growth approximation is developed to model the nanocrystallization kinetics. Results yield Avrami exponent values near to 1 at low transformed volume fraction, which decrease as the crystalline fraction increases. The compositional dependence of the nanocrystalline microstructure achieved after primary crystallization is also modelled. Two different nucleation phenomena are considered: either in contact with an already formed crystallite, or in isolated regions. Results from the simulations are compared with experimental data for FeCoNbB alloys and a good qualitative agreement is found

*Corresponding author: Prof. A. Conde

Departamento de Física de la Materia Condensada. Universidad de Sevilla.

Apartado 1065, 41080 Sevilla (Spain).

Phone: (34) 95 455 28 85

Fax: (34) 95 461 20 97

E-mail: conde@us.es

1   Introduction

Amorphous and nanocrystalline alloys have attracted much attention from the research community since the works of Duwez on AuSi [1] and Yoshizawa on FINEMET [2]. Besides the interest provoked by the fundamental physics underlying in such microstructures, technological applicability of amorphous and nanocrystalline alloys has been profusely explored due to the outstanding properties achieved, overcoming those of their conventional crystalline counterparts (e.g. mechanical, for Al-based alloys [3]; magnetic, for Fe-based alloys [4], etc).

Nanocrystalline alloys obtained from primary crystallization of a precursor amorphous alloy exhibit a microstructure formed by small crystallites (~10 nm in size) embedded in a residual amorphous matrix. Two big families can be identified: Fe-based [4] and Al-based alloys [3]. The former are interesting due to their magnetic properties and the latter, due to their mechanical ones. The following discussion will correspond to Fe-based alloys, although it could be easily extended to Al-based alloys and other families.

The typical composition of Fe-based nanocrystalline alloys is Fe-M-ET-(Cu), where M is a metalloid and ET is an early transition metal. The addition of metalloids (B, P, Si) is necessary to obtain a precursor amorphous alloy by rapid quenching techniques. The early transition metals (Zr, Nb, Hf, Mo) have, if any, a very low solubility in the α-Fe phase and, consequently, will be expelled out to the amorphous matrix. However, due to the very slow diffusivity of these elements in the amorphous phase, they pile up at the crystal–matrix interface constraining the growth of the crystalline phase to the nanocrystalline scale. This phenomenon is responsible for the development of a nanocrystalline microstructure by primary crystallization of a precursor amorphous alloy.

The addition of Cu is not necessary to obtain nanocrystalline microstructure in some compositions named NANOPERM [5] but, generally, refines the microstructure through the formation of Cu-rich clusters previous to the nanocrystallization [6]. This phenomenon is also responsible for the fine nanocrystalline microstructure observed in FINEMET alloys [4].

Several compositional modifications have been proposed to improve the applicability of nanocrystalline alloys. For example, in 1998 [7], HITPERM alloys were obtained after partial Fe substitution for Co to extend up to higher temperatures the soft magnetic properties of nanocrystalline alloys. In such systems, Co concentration was found to be homogeneous throughout the amorphous matrix and the nanocrystals [8,9]. It was also found that Cu addition yields a refinement of the microstructure for Nb-HITPERM alloys [10] but was useless for Zr-HITPERM alloys [8]. The microstructure observed for Cu-free NANOPERM [11] and HITPERM [8,10] alloys (with a concentration of ET >5 at.%) consists on very irregular nanocrystals, which can be described as agglomerates of smaller and more regular units (~5 nm) with the same crystallographic orientation [10]. This microstructure can be understood as the result of the competition of two different nucleation phenomena: either in isolated regions, or in contact with a crystallite. The former has the advantage of nucleating in a region rich in Fe, but the interface energy between the nucleus and the surrounding amorphous is high. In the latter nucleation phenomenon, which could be also understood as epitaxial growth, the interface energy of the new nucleus is smaller but the region might have a lower Fe concentration. The size of the small units forming the crystalline agglomerates is almost constant along the crystallization process (e.g. ~5 nm for Nb-containing HITPERM alloys [10]). This fact, along with some recent results on the isothermal nanocrystallization kinetics [12], enables to consider an instantaneous growth

approximation to describe the nanocrystallization process of such systems. This approximation implies that the time required for a new nucleus to grow up to ~5 nm in diameter is neglected in comparison with the time required for the full nanocrystallization process.

Several computer simulations procedures have been applied to study the crystallization process, among them Montecarlo [13,14] and molecular dynamics [15] can be found. Cellular automata has also been applied to describe several crystallization processes [16,17,18,19,20] and results obtained have been compared to Johnson-Mehl-Avrami-Kolmogorov (JMAK) theory [21,22,23] predictions. Cellular automata modellizations consist on a discretization of the time and the space in order to apply evolution laws. Generally, the character of the evolution of the system is deterministic, i.e. the configuration of the system at a time step τ is univocally determined by the configuration at the time step τ-1. The application of these methods to crystallization processes is straightforward for growth processes but nucleation is a probabilistic phenomenon and this feature must be taken into account. Some authors choose an initial distribution of pre-nuclei, which can be active since the beginning of the process or retarded and being activated at a predetermined time step [16], neglecting the probabilistic character of the nucleation process and limiting the study to the deterministic effect of a growth process and its dependence with the nucleation density. Other authors [17,18] directly assume this probabilistic character of the nucleation process randomly choosing a set of sites to nucleate at each time step τ among those which are able to nucleate (e. g. grain boundaries in recrystallization).

The aim of this paper is to show that an instantaneous growth approximation can properly describe the nanocrystallization kinetics and the microstructure developed during this process. This will be done using a cellular automata simulation program: a

three dimensional space is divided in cubic cells and the time is discretized in iteration steps. The process to be described in the present paper considers the nucleation phenomenon alone in a homogeneous amorphous matrix, neglecting the growth process. Therefore, every cell is suitable to nucleate but in order to do so it must fulfil not only deterministic requisites but the stochastic character of nucleation has to be taken into account. This is considered by randomly selecting a cell as candidate to develop a new crystalline nucleus. This nucleus will yield a nanocrystal only after fulfilling some deterministic and probabilistic requisites, which depend on the characteristic parameters of this cell and its neighbourhood: volume available for nucleation, surface energy developed between the eventual new nucleus and its environment, and composition of the region where the nucleus would be formed.

2 JMAK theory

Crystallization of metallic amorphous alloys can be described by nucleation and growth processes [24]. These transformations are generally described by the JMAK theory, which describes the time evolution of the transformed fraction, X, as:

$$X = 1 - \exp\left[-\left(k \cdot (t - t_0)\right)^n\right] \tag{1}$$

where k is the frequency factor, t is the time, t_0 is the induction time and n is the Avrami exponent. From the latter parameter, it is possible to extract information about the phenomena involved in the crystallization process as [24]:

$$n = n_I + d \cdot n_G \tag{2}$$

where n_I is ascribed to nucleation process, being 1 for a constant nucleation rate, below 1 for a decreasing nucleation rate and above 1 for an increasing nucleation rate; d is the dimension of the growth; and n_G is ascribed to the growth process, being ½ for diffusion controlled growth and 1 for interface controlled growth [24].

Although JMAK theory was developed for polymorphic transformations during isothermal regimes, its application has been successfully extended to transformations involving compositional changes [25,26] and non-isothermal regimes [27,28,29]. JMAK theory takes into account the geometrical overlapping between growing crystals as the only effect to slow down the crystallization process with the increase of transformed volume and, assuming a constant nucleation rate, n=2.5 for a three dimensional diffusion controlled growth and n=4 for a interface controlled three dimensional growth. However, in the case of nanocrystallization processes, this effect alone can not describe the transformation and values of Avrami exponent below 1 can be found [4,12,25,26,27,30]. The responsible for these low values of n can be the blocking of the crystal growth as ET atoms pile up at the edge of the nanocrystals. Although this constraining effect is not considered in JMAK theory, a general qualitative description considers the presence of a strongly inhibited growth process and a progressive exhaustion of nucleation sites. The instantaneous growth approximation neglects the time a certain nucleus needs to grow up to its limit value, at which it is blocked by the wall of rejected ET atoms. Therefore, $n_G = 0$, and expression (2) should be simplified to:

$$n = n_I \tag{3}$$

Under this approach, each formed nucleus would reach instantaneously its final size and following growth processes are banned. Previous experimental studies using this approach allowed to extract detailed information on the nanocrystallization kinetics of Nb-containing HITPERM alloys [12].

3   Model program

In terms of the different partitioning of the elements during nanocrystallization, a typical Fe-based composition should be $Fe_xSol_yExc_{100-x-y}$; where Sol identifies the elements which are soluble in the α-Fe (e.g. Co, Si, Ge…) and Exc identifies the elements which are excluded from the crystalline phase and expelled out to the residual amorphous matrix (Nb, Zr, B, …). The composition of the crystalline phase would be $Fe_{100-y}Sol_y$ and that of the residual amorphous phase could be obtained from the balance equation:

$$Fe_xSol_yExc_{100-x-y} = X_C (Fe_{100-y}Sol_y) + (1-X_C) Fe_uSol_yExc_z \qquad (4)$$

where X_C is the crystalline volume fraction. If there is a preferential partitioning of an element to the crystals or to the amorphous phase, a convenient selection of the y index (the concentration of elements different to Fe in the crystalline phase) can take it into account.

The model used in these experiments describes a three dimensional space formed by cubic cells. Following the microstructure observed for NANOPERM and HITPERM alloys and the two nucleation mechanisms considered to describe this microstructure ("in contact" and "isolated" nucleations), each cell is characterized by three parameters: occupation (*Occ*), composition (*C*) and order (*Ord*).

- The occupation parameter takes three possible numeric values, indicating whether the cell is a crystalline unit (*Occ*=2), or it is amorphous but in contact with an already formed crystal (*Occ*=1), or isolated (*Occ*=0).

- The composition indicates the Fe concentration in the cell.

- The order is a number assigned to each nucleus formed in isolated regions by order of appearance. This nucleus will form an agglomerate of crystallites whose components will have a common value of the parameter *Ord*.

At the beginning, all the cells of the space are set to isolated value for occupation, to the nominal value of Fe concentration (C = x) for composition and to zero for the order number, as no crystallite is formed and the initial composition is supposed to be homogeneous.

A flow diagram corresponding to one iteration step of the program proposed to resemble an instantaneous growth crystallization process is schematically shown in figure 1. For each iteration step, a cell is randomly chosen and tested against several deterministic and probabilistic requisites. If all these requisites are fulfilled, the cell will nucleate leading to a new crystallite. However, if any requisite is not fulfilled, the cell will not nucleate and will be discarded for further considerations, starting the process again.

3.1   *Considering the occupation of the cell*

The first stage of each iteration step of the process is to randomly choose a cell and to check its occupation value. If this value indicates that the cell is already nucleated (*Occ*=2), the cell is discarded for further considerations, an iteration step is counted and a new cell is chosen. Once the chosen cell fulfils the deterministic condition of being amorphous, the effect of a reduction in the surface energy for "in contact" nucleation compared to "isolated" nucleation is considered using the value of *Occ* and following expression:

$$Occ + Rnd > \sigma \qquad\qquad (5)$$

where *Rnd* is a random number from 0 to 1 and σ is a parameter related with the surface energy. A value of σ=0 would indicate no energetic advantage for nucleation "in contact" with respect to "isolated" nucleation (every amorphous cell with *Occ*=0 or 1 will fulfil the requisite expressed in the previous equation). A value of σ>1 would ban

the nucleation in isolated regions. If the condition required in equation (5) is not fulfilled, the cell is discarded for further considerations, an iteration step is counted and a new cell is chosen.

3.2   Considering the composition of the environment

When all the previous requisites have been satisfied, the composition of the chosen cell and that of the neighbourhood must be considered. In order to build a crystalline cell, its Fe concentration must increase to reach a certain value (100-y). Therefore, Fe must replace the elements Exc (non soluble in the α-Fe phase). A first step would be to check if the neighbourhood of the chosen cell is rich enough in Fe to supply the concentration needed by the chosen cell. At this point, it is worth noticing that the instantaneous growth approach used throughout this paper is based on the assumption that the distances for diffusion are very short (due to the blocking effect of ET atoms). Therefore, the volume available to the forming nucleus to extract Fe from the surrounding cells might be limited. In the present study, a maximum volume is considered as 6 times that of the cell (corresponding to the six neighbour cells, assuming Von Neumann neighbourhood [16]) but a parameter, *vol*, is defined to take into account the possibility of a reduction of the affected volume by the formation of a new crystallite. As an example, it can be considered the volume of the smallest sphere in which the cubic cell is contained, which has a radius $\sqrt{3}/2$ times the length of the side of the cubic cell. The value of *vol* in such a case would be 1.72, which is the difference between the volume of the sphere and that of the cubic cell. This volume would be equally divided among the six neighbour cells.

If the Fe concentration available in the volume *vol* is less than the needed, this cell cannot nucleate (deterministic condition) and it would be discarded for further considerations, an iteration step would be counted and a new cell would be chosen.

The probabilistic character of nucleation is also associated with that of compositional fluctuations. Therefore, there is a probability for the nucleus to form depending on the richness of the surrounding cells in Fe, P_{NUC}, which could be considered as:

$$P_{NUC} = 1 - \exp\left(-C_{av}/C_{need}\right)$$

(6)

where C_{av} is the concentration of Fe available in the *vol* volume surrounding the cell and C_{need} is the concentration of Fe needed in the chosen cell. In order to allow the chosen cell to nucleate, P_{NUC} is compared with a randomly generated number *Rnd'* and the requisite will be considered fulfilled if P_{NUC}>*Rnd'*.

3.3   Nucleation

Once every previous requisite has been fulfilled, the nucleus will be formed. The parameters of the chosen cell as well as those of the neighbour cells will be redefined.

- The occupation number will be 2 for the new crystallite unit and 1 for all the neighbour cells which were not already nucleated.

- The Fe concentration given to the nucleated cell will be equally shared between the six neighbour cells. However, it is possible that some of the neighbour cells contain less amount of Fe than the average they should supply to the chosen cell (e.g. the neighbour cells which were already crystalline cannot supply Fe to the forming nucleus). In such a case, the neighbour with a poor concentration in Fe would give all its Fe content to the forming nucleus (or zero in the case of a

crystalline neighbour cell) and the rest of the needed concentration will be shared among the other neighbour cells.

- If the occupation number of the chosen cell was 1 ("in contact" nucleation) the order number will be that of the neighbour cell already nucleated (if there are more than one crystallized neighbour cell, the parent cell is randomly chosen among them). If the occupation number was 0, a new order number is assigned.

The procedure is repeated a selected number of steps, deciding each time whether the chosen cell is nucleated or discarded as described above.

4   Results from the program

After a selected number of iteration steps, the crystalline fraction, X_C, calculated as the ratio between the number of steps yielding a nucleation process and the total number of cells, is extracted in order to visualize the progress of the instantaneous growth process. The number of iteration steps between two data point acquisitions corresponds to one tenth of the total number of cells. This allows a good resolution of the modelled curve and that the information contained in each data point to be representative of a global evolution of the system. The chosen number of iteration steps was $3 \cdot 10^6$ s for all the simulations performed, which allows reaching the saturation of the process and can be considered as a measure of time.

In order to apply equation (1) to non polymorphic transformations, it is necessary to define a normalized transformed fraction, X, from X_C as:

$$X = \frac{X_C}{X_C^{MAX}}$$

(7)

where X_C^{MAX} is the maximum value of X_C. In the model proposed, the value of X_C^{MAX} is

that which would lead to an exhaustion of Fe in the amorphous matrix, banning the

formation of new nuclei:

$$X_C^{MAX} = \frac{x}{100 - y} \qquad (8)$$

Thus the ln(-ln(1-X)) versus ln(t) curve (JMAK plot) can be calculated and the

Avrami exponent, n, can be obtained as the slope of this curve. Figure 2 shows two

examples of the curves obtained for a $Fe_{60}Sol_{18}Exc_{22}$ alloy composition in a space of

100^3 cells, with σ=0.5 for two different values of *vol*: 1.72 and 6 cells. Curves of $X(t)$

are shown in figure 2a, the well known two slopes behaviour of the JMAK plot reported

for nanocrystallization kinetics [12,25,26,30,31] is clearly observed in figure 2b. Figure

2c shows the corresponding local Avrami exponent. As the available volume (*vol*) to

extract Fe increases, the modelled process is accelerated and the final crystalline volume

fraction increases. This feature could be compared with the effect of temperature on

isothermal annealing processes: as the temperature increases, atomic diffusion is

enhanced, increasing the region affected by the formation of a new crystallite and the

final crystalline volume fraction also increases [12,32,33,34,35]. The evolution of

obtained values of n is in agreement with JMAK theory predictions assuming an

instantaneous growth process ($n_G = 0$). At the beginning, $n \sim 1$ because the probability

for nucleation is not affected by the nucleation of just few cells, being nucleation in

isolated regions the only significant contribution to the crystallization. However, as the

number of nucleated cells increases, an increase of n is clearly observed due to the

contribution of the second mechanism of nucleation (in contact with an already formed

crystalline cell). Finally, n decreases because the number of cells suitable for nucleation

is reduced due to both the decrease in Fe concentration and the increase of the number

of cells already nucleated. As *vol* increases, the maximum value of *n* increases: the available Fe concentration for a new crystallite increases and, therefore, the effect due to the decrease in Fe concentration is observed at higher values of X_C.

Figure 3 shows the effect of the parameter σ (from 0 to 0.9) on the crystalline fraction, on the JMAK plot and on the local Avrami exponent. For $\sigma = 0$, the nucleation "in contact" with a previously formed crystallite is not favoured by a reduction in the interface energy. Consequently, the Avrami exponent continuously decreases from $n = 1$ (Fig. 3c), as there is no reason for any enhancement of the nucleation frequency during the nanocrystallization process. This could simulate the nanocrystallization process occurring in some ~1 at. % Cu-added Fe based alloys [36], for which lower values of *n* are observed at low crystalline volume fractions in comparison with those of similar alloy compositions without Cu [27]. In these alloys, the Cu clustering phenomenon previous to the nanocrystallization supplies sites randomly distributed throughout the matrix for heterogeneous nucleation of the α-Fe phase. However, it must be taken into account that the size of the Cu clusters is much smaller than that of the crystallite units [9,36] and the representation of equal size cells used in this simple model would underestimate the probability of a nucleus to be form in contact with a Cu cluster. As σ increases, it is evidenced that the maximum of *n* increases, as the mechanism of nucleation in contact with an already formed crystal is progressively favoured by the increase in number of crystallites.

The model can consider compositional effects as well. Figure 4 shows two examples of (a) crystalline volume fraction evolution, (b) the JMAK plot and (c) the local Avrami exponent obtained for two $Fe_xSol_{78-x}Exc_{22}$ alloys (x=18 and 60) in a space of 100^3 cells, with σ=0.5 and *vol*=1.72. The decrease of the concentration of Fe yields a strong impoverishment of Fe at the vicinity of a formed crystal. This fact decreases the

probability of the nucleation mechanism "in contact" with an already formed crystallite, as the required enrichment of the cell in Fe is large in comparison with the Fe concentration in the available volume, *vol*, (a variation of this parameter modifies the numerical but not the qualitative results). Therefore, P_{NUC} is very small and, consequently, the nanocrystallization process is slowed down: at a given number of iteration steps, the crystalline volume achieved is much smaller for $x = 18$ than for $x = 60$ (see Fig. 4a). For 18 at. % Fe alloy, the impoverishment in Fe of the region close to an already formed nanocrystal is responsible for the absence of the initial increase of *n* observed for the 60 at. % Fe alloy, although the surface energy would be lower for "in contact" nucleation compared to "isolated" one for both alloys.

Properly using the three parameters assigned to each cell, it is possible to extract further information from the simulation program: e.g. the distribution of size of the agglomerates and some simulated images or compositional maps. Figure 5a shows, for the two alloys of figure 4, the evolution of the average size *<D>* of the crystalline agglomerates (crystalline units formed in contact and thus with the same crystallographic orientation), calculated as:

$$< D >=< N >^{1/3} \tag{9}$$

where *<N>* is the average number of cells forming an agglomerate (number of nucleated cells divided by the number of agglomerates).

Figure 5b shows the size distribution of agglomerates after 10^6 iteration steps. It is clear that a decrease in Fe content yields a decrease in size of the agglomerates. In the case of 18 at. % Fe, it can be observed that the maximum number of cells in an agglomerate is 3 $(D=\sqrt{3})$, whereas for 60 at. % Fe alloy, there are agglomerates containing more than 30 cells $(D>\sqrt{30})$.

5   Comparison with experimental data

The kinetic results obtained from the proposed model can be compared to experimental results on the nanocrystallization kinetics of amorphous alloys. As an example, figure 6 shows the experimental results on the nanocrystallization process of $Fe_{60}Co_{18}Nb_6B_{16}$ alloy. Time dependence of the crystalline volume fraction was measured using differential scanning calorimetry registering the heat flow during an isothermal annealing at 743 K (26 K below the onset of crystallization). In order to calculate X, the maximum value of X_C was obtained from the total enthalpy released during non-isothermal scans and the induction time 85 s was obtained from the intersection of the steepest slope of X_C vs. time. Details were reported elsewhere [12]. Although valuable comparisons between the qualitative behaviour of experimental and model systems can be made, the absolute values of the crystalline volume fraction cannot be directly compared with the results obtained from the model, as the minimum distance at which a new nucleus is considered isolated is arbitrarily chosen equal to the diameter of the crystalline unit in order to simplify the calculations.

The experimental curves at the very beginning of the nanocrystallization process are affected by the induction time, which is the time required to activate the process and depends on the temperature. In the model proposed, there is no time required for activating the process, thus induction time is not considered and experimental values at times of the order of the induction time might not be modelled. In order to avoid this confusion, plots of figure 6b and 6c were marked with a thicker line for points satisfying the condition:

$$t\text{-}t_0 > 2 \cdot t_0 \tag{10}$$

Apart from the differences between the experimental and the model results pointed above, a good agreement can be found between them. At low values of

15

crystalline volume fraction, the Avrami exponent is close to 1. Its increase at this stage

can be ascribed to the triggering of "in contact" nucleation mechanism by the increase

in number of crystallites able to supply sites for this heterogeneous nucleation. As

crystalline volume fraction increases, the Avrami exponent decreases due to the

decrease in the number of available places for new nuclei. No explanation in the frame

of Johnson-Mehl-Avrami-Kolmogorov theory was previously found for these low

values of Avrami exponent, close to 1, observed for the nanocrystallization processes

and some modifications were proposed to explain them [25,26,32,37,38]. However, an

instantaneous growth approximation can yield these low values, as it was shown above,

the Avrami exponent would be $n = n_I$. A value of $n_I > 1$ would indicate an increasing

nucleation frequency and $n_I < 1$ a decreasing nucleation frequency.

Properly using the parameter *Ord* ascribed to each cell, it is possible to build

compositional maps and simulate two-dimensional images which could be compared

with experimental images of nanocrystalline alloys obtained by transmission electron

microscopy (TEM). Figure 7 and 8 show such compositional maps as a function of the

number of iterations, for a selected 10x10 cells plane of the 100^3 cells space used in the

simulation, for two $Fe_xSol_{78-x}Exc_{22}$ alloys ($x= 60$ and 18, respectively). These two

modelled alloys could be compared to the real $Fe_{60}Co_{18}Nb_6B_{16}$ and $Fe_{18}Co_{60}Nb_6B_{16}$

alloys, respectively. TEM images of such alloys, obtained at different times of

annealing at 35 K below the onset of crystallization are also shown in figures 7 and 8,

respectively.

Both simulated and experimental images agree describing a continuous

nucleation process (the number of crystalline units continuously increases). In the case

of the alloy with 60 at. % Fe, agglomerates appears since the very beginning and

although their size increases, the size of their crystalline units is almost independent of

the annealing time. In the case of 18 at. % Fe alloy, there are no agglomerates and the only difference as the nanocrystallization progresses is the increase in number of small regular crystallites ~5 nm in size.

Conclusions

The cellular automata simulation program proposed in the present paper is based on an instantaneous growth approximation. In this frame, the time required for a nucleus to grow up to its maximum size is neglected in comparison with the time required for the crystallization process.

This simulation yields to the well known and experimentally observed two slopes behaviour of the JMAK plots. The local Avrami exponent obtained from the simulations resembles the experimental results obtained for the kinetics of nanocrystallization, consisting on an Avrami exponent ~1 for low values of the transformed fraction, which decreases as the crystalline volume fraction increases.

In the frame of an instantaneous growth approximation, results can be described by the JMAK theory. The Avrami exponent, $n=n_I$, accounts only for nucleation processes as $n_G=0$. Therefore, $n=1$ indicates a constant nucleation frequency, $n>1$ indicates an increasing nucleation frequency and $n<1$ a decreasing nucleation frequency.

Compositional dependence of the microstructure achieved in nanocrystalline alloys is reproduced considering two different nucleation phenomena: in contact with an already formed crystallite and in isolated regions.

Model predictions were compared with experimental results on FeCoNbB alloys and a good qualitative agreement was found for the compositional dependence of nanocrystallization kinetics and the microstructure developed during the process.

Acknowledgements

References

[1]   Klement W Jr., Willens RH, Duwez P, Nature 1960; 187: 869.
[2]   Yoshizawa Y, Oguma S, Yamaguchi K J Appl Phys 1988; 64: 6044.
[3]   Inoue A, Prog Mater Sci 1998; 43: 365.
[4]   McHenry ME, Willard MA, Laughlin DE, Prog Mater Sci 1999; 44: 291.
[5]   Suzuki K, Makino A, Kataoka N, Inoue A, Masumoto T, Mater Trans JIM 1991; 32: 93.
[6]   Suzuki K, Makino A, Inoue A, Masumoto T, J Appl Phys 1991; 70: 6232.
[7]   Willard MA, Laughlin DE, McHenry ME, Thoma D, Sickafus K, Cross JO, Harris VG, J Appl Phys 1998; 84: 6773.
[8]   Ping DH, Wu YQ, Hono K, Willard MA, McHenry ME, Laughlin DE. Scr Mater 2001; 45: 781.
[9]   Zhang Y, Blázquez JS, Conde A, Warren PJ, Cerezo A. Mater Sci Eng A 2003; 353: 158.
[10]   Blázquez JS, Franco V, Conde A, J Phys Cond Matter 2002; 14: 11717.
[11]   Makino A, Hatanai T, Inoue A, Masumoto T, Mater Sci Eng A 1997; 226-228: 594.
[12]   Blázquez JS, Millán M, Conde CF, Conde A, Phil Mag 2007 (in press)
[13]   Muller SF, Nanostruc Mater 1995; 6: 787.
[14]   Zheng YG, Lu C, Mai YW, Gu YX, Zhang HW, Chen Z, Appl Phys Letters 2006; 88: 144103.
[15]   Yamakov V, Wolf D, Phillpot SR, Gleiter H, Acta Mater 2002; 50: 5005.
[16]   Hesselbarth HW, Göbel IR, Acta Metall Mater 1991; 39: 2135.
[17]   Goetz RL, Scripta Mater 2005; 52: 851.
[18]   Kugler G, Turk R, Comp Mat Sci 2006; 37: 284.
[19]   Ding HL, He YZ, Liu LF, Ding WJ, J Cryst Growth 2006; 293: 489.
[20]   Mukhopadhyay P, Loeck M, Gottstein G, Acta Mater 2007; 55: 551.
[21]   Kolmogorov AN. Bull Acad Sci USSR, Phys Ser 1937; 1: 355.
[22]   Johnson WA, Mehl RF, Trans Am Inst Mining Met Engrs 1939; 135: 416.
[23]   Avrami M, J Chem Phys 1941; 9: 177.
[24]   Christian JW, in: The Theory of Transformation in Metals and Alloys, Part 1, Pergamon, Oxford, 1975, p. 542.
[25]   Clavaguera-Mora MT, Clavaguera N, Crespo D, Pradell T, Prog Mat Sci 2002; 47: 559.
[26]   Claudio D, González-Hernández J, Licea O, Laine B, Prokhorov E, Trapaga G, J Non-Cryst Solids 2006; 352: 51.
[27]   Blázquez JS, Conde CF, Conde A, Acta Mater 2005; 53: 2305.
[28]   Vázquez J, Barreda DG, López-Alemany PL, Villares P, Jiménez-Garay R, J All Compd 2006; 421: 109
[29]   Farjas J, Roura P, Acta Mater 2006; 54: 5573.
[30]   Blázquez JS, Conde CF, Conde A, Appl Phys A 2003; 76: 571.
[31]   Illekova E, Thermochim Acta 2002; 387: 47.
[32]   Lecaude N, Perron JC, Mater Sci Eng A 1997; 226-228: 581.
[33]   Conde CF, Conde A, Mater Letters 1994; 21: 409.
[34]   Borrego JM, Conde CF, Millán M, Conde A, Capitán MJ, Joulaud JL, Nanostr Mater 1998; 10: 575.
[35]   Conde CF, Millán M, Borrego JM, Conde A, Capitán MJ, Joulaud JL, Phil Mag Letters 1998 ; 78 : 221.

[36]   Hono K, Prog Mater Sci 2002; 47: 621.
[37]   Kristiakova K, Svec P, Phys Rev B 2001 ; 64 : 184202
[38]   Hermann H, Mattern N, Roth S, Uebele P, Phys Rev B 1997; 56: 13888.

Figure captions

Figure 1: Flow diagram of the simulation program.

Figure 2. (a) Crystalline fraction versus iteration steps, (b) JMAK plot and (c) Avrami exponent calculated for a $Fe_{60}Sol_{18}Exc_{22}$ alloy: σ=0.5 and *vol*=1.72 (blue) and 6 (red).

Figure 3. (a) Crystalline fraction versus iteration steps, (b) JMAK plot and (c) Avrami exponent calculated for a $Fe_{60}Sol_{18}Exc_{22}$ alloy: *vol*=1.72 and σ=0, 0.5 and 0.9.

Figure 4. (a) Crystalline fraction versus iteration steps, (b) JMAK plot and (c) Avrami exponent calculated for a $Fe_xSol_{78-x}Exc_{22}$ alloy (x= 60 and 18): σ=0.5, *vol*=1.72.

Figure 5. (a) Average size of the agglomerates versus the iteration step number and (b) agglomerate size distribution after $3 \cdot 10^6$ iteration steps for a $Fe_xSol_{78-x}Exc_{22}$ alloy (x= 60 and 18). In both, σ=0.5, *vol*=1.72.

Figure 6. (a) Crystalline volume fraction versus time minus the induction time, (b) JMAK plot and (c) Avrami exponent obtained for a $Fe_{60}Co_{18}Nb_6B_{16}$ alloy during isothermal annealing at 743 K. The thick line in (b) and (c) marks the values obtained for $t-t_0 > 2t_0$ (t_0=85 s).

Figure 7. Plane images simulated by the model for a $Fe_{60}Sol_{18}Exc_{22}$ alloy after different iteration steps compared with TEM images of nanocrystalline samples of $Fe_{60}Co_{18}Nb_6B_{16}$ alloy annealed different times at 716 K. In the simulated image obtained after 10^6 iteration steps, the number indicate the order of formation of the different agglomerates.

Figure 8. Plane images simulated by the model for a $Fe_{18}Sol_{60}Exc_{22}$ alloy after different iteration steps compared with TEM images of nanocrystalline samples of $Fe_{18}Co_{60}Nb_6B_{16}$ alloy annealed different times at 686 K.
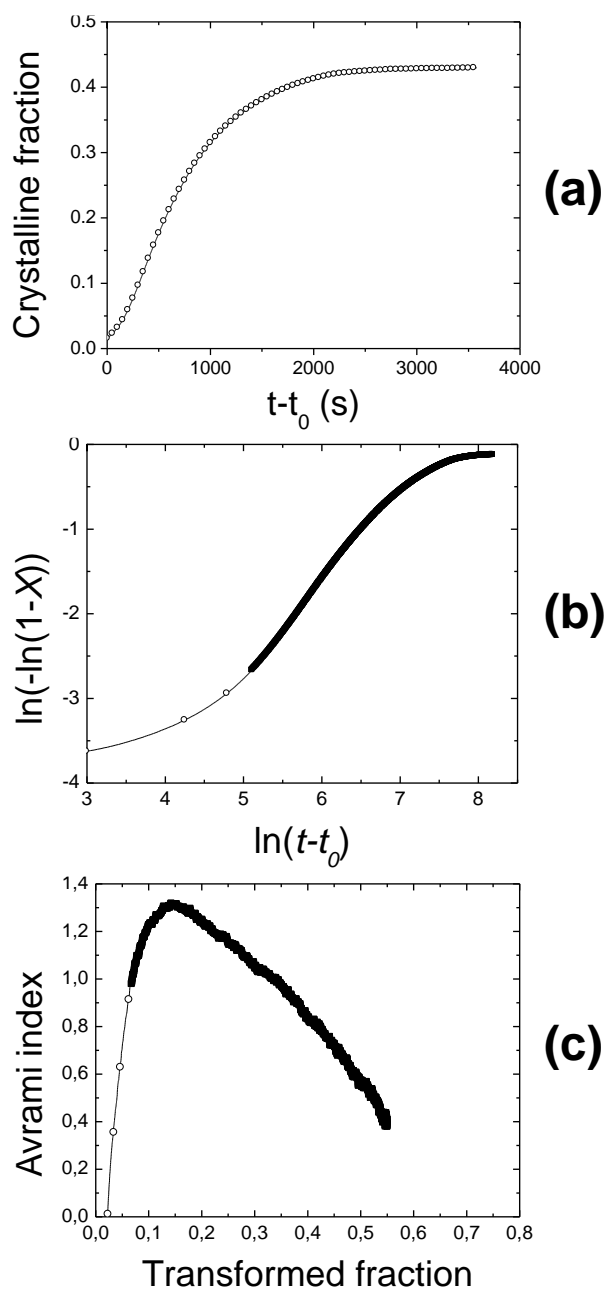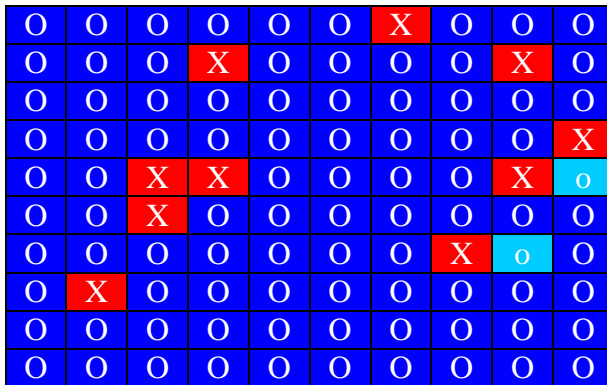
Figure 1
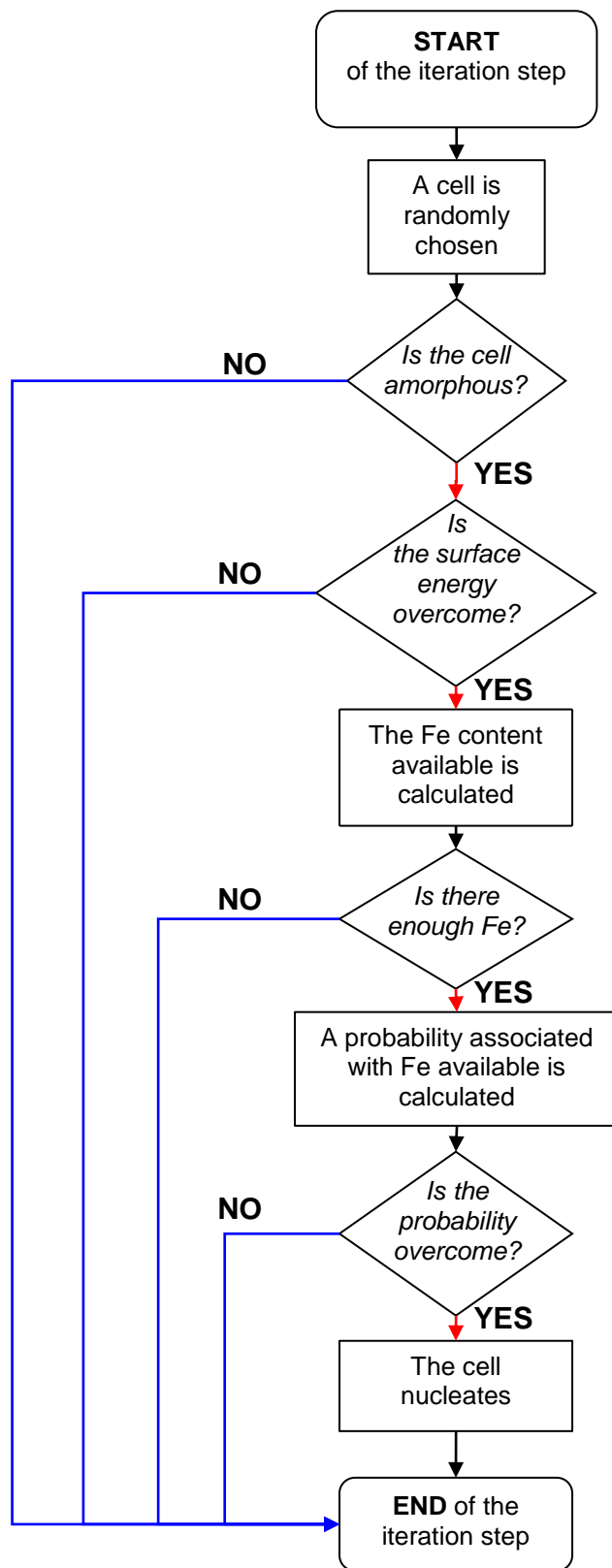
Figure 2
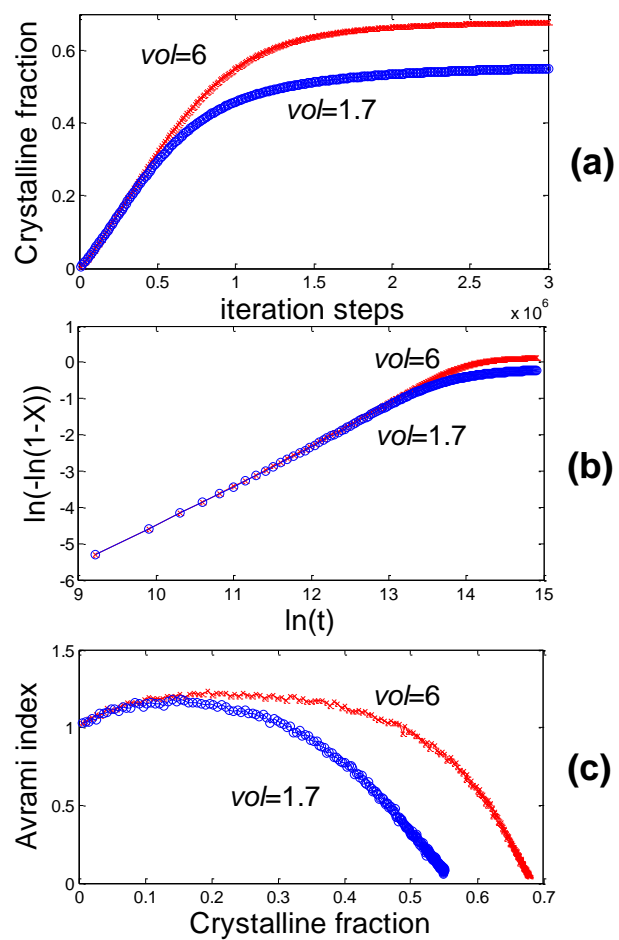
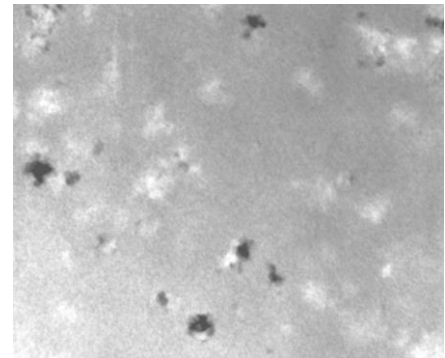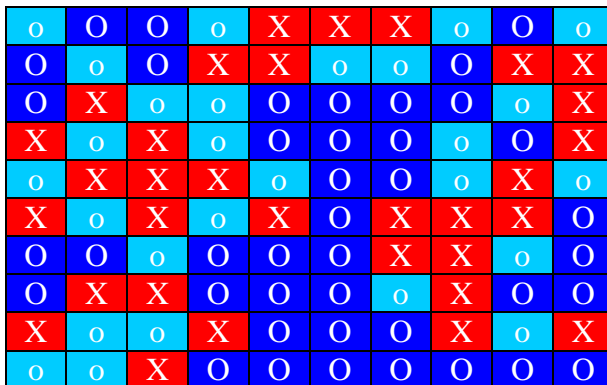Figure 3
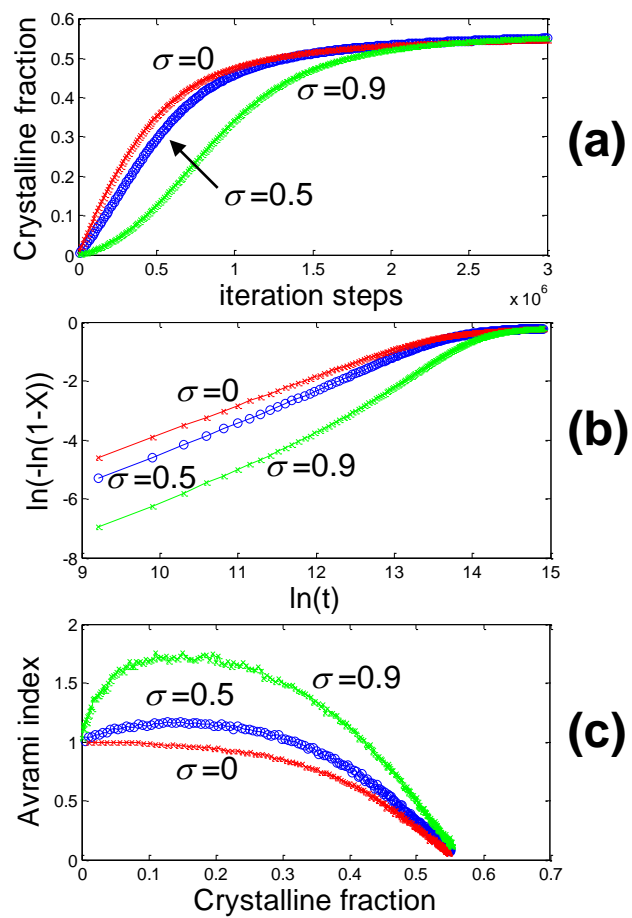
Figure 4
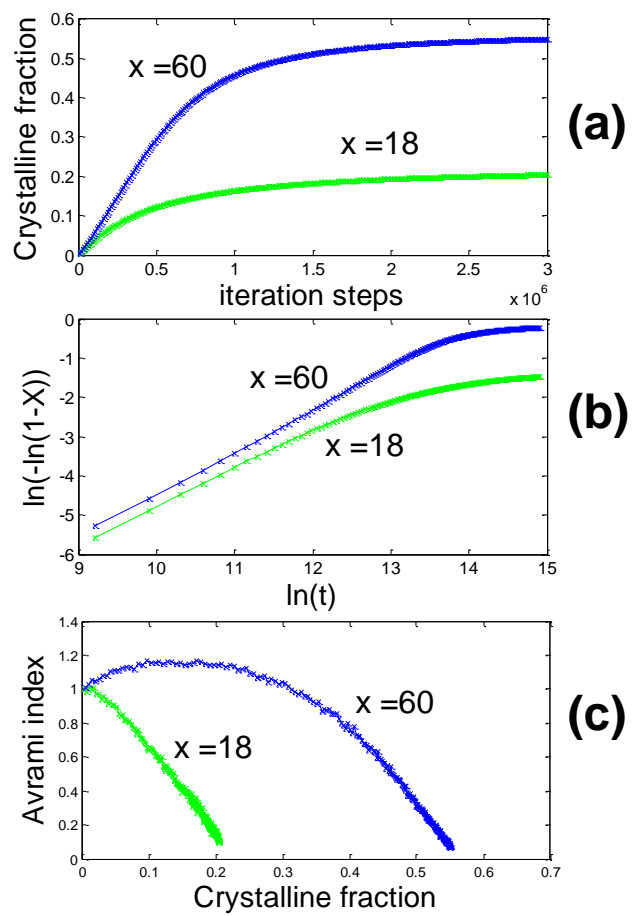
Figure 5
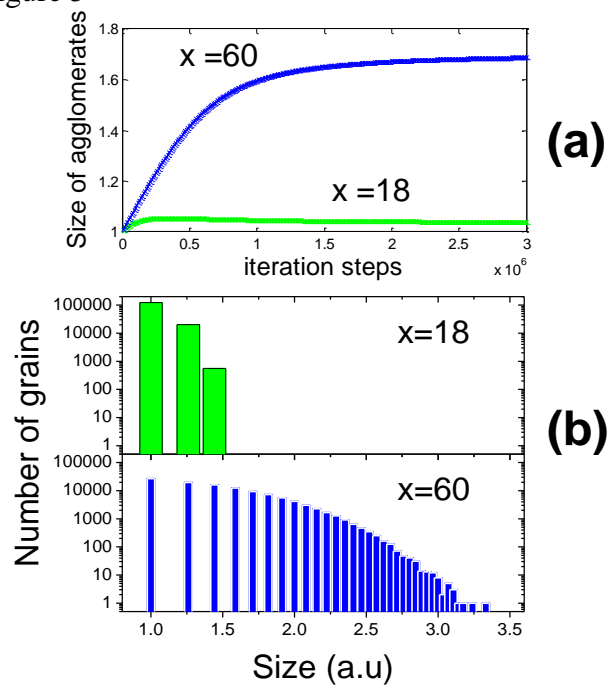
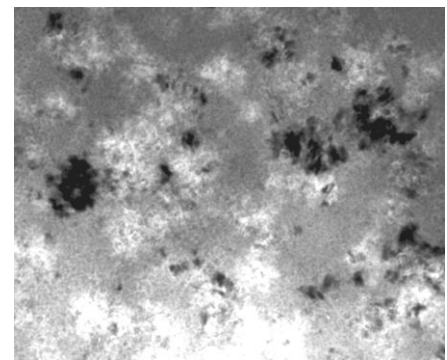Figure 6

Figure 7

10^5 iteration steps
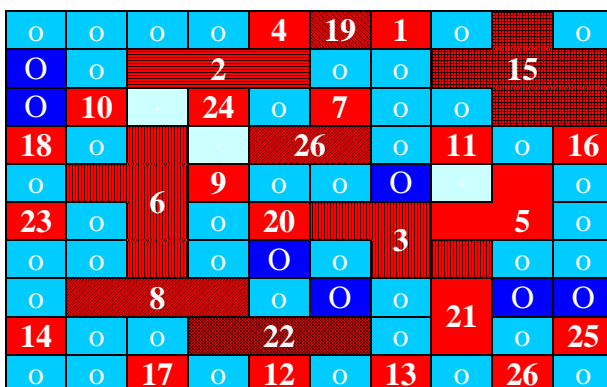
0.5 h at 716 K

$5 \cdot 10^5$ iteration steps
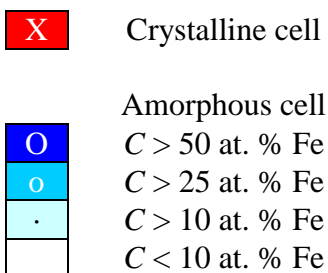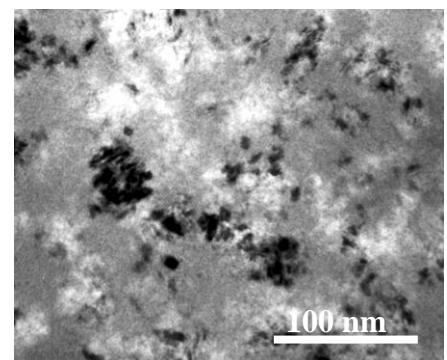
5 h at 716 K

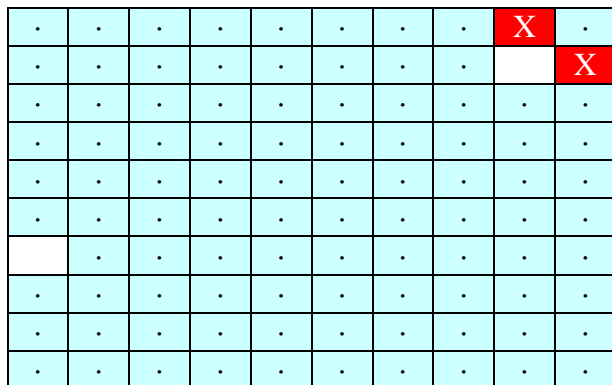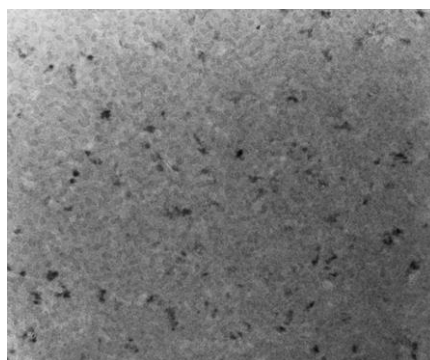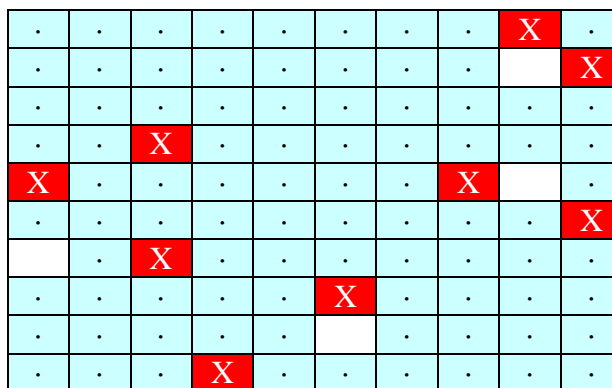10^6 iteration steps

12.5 h at 716 K

| X | Crystalline cell |

Amorphous cell

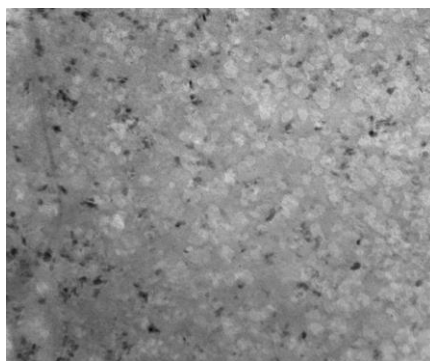| O | $C > 50$ at. % Fe |
o	$C > 25$ at. % Fe
·	$C > 10$ at. % Fe
	$C < 10$ at. % Fe

Figure 8

10^5 iteration steps

0.5 h at 686 K

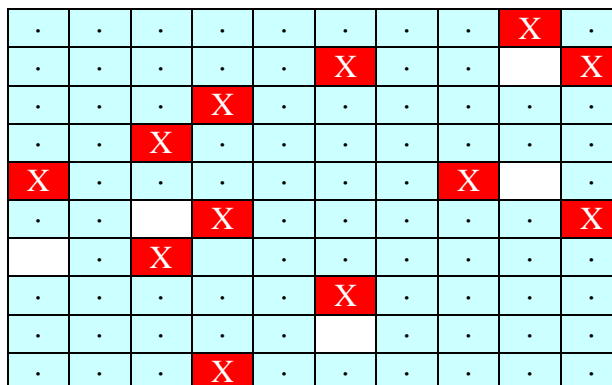
5·10^5 iteration steps

5 h at 686 K

10^6 iteration steps

12.5 h at 686 K

| X | Crystalline cell |

Amorphous cell

O	$C > 50$ at. % Fe
o	$C > 25$ at. % Fe
·	$C > 10$ at. % Fe
	$C < 10$ at. % Fe